



Swelling behavior study of poly(methacrylic acid-co-acrylamide) nano-composite hydrogel adsorbents containing different nanoparticles

Seyed Jamaledin Peighambaroust^{a,*}, Hamid Safarzadeh^b

^aFaculty of Chemical and Petroleum Engineering, University of Tabriz, Tabriz, 5166616471, Iran, email: j.peighambaroust@tabrizu.ac.ir

^bSeparation Processes and Nanotechnology Lab., Faculty of Caspian, College of Engineering, University of Tehran, Tehran, Iran, email: hamidsafarzade1993@gmail.com

Received 24 November 2022; Accepted 25 May 2023

ABSTRACT

The degree of swelling can be an essential issue in comparing hydrogels in different studies. In this study, the swelling effect of hydrogel has been investigated. Poly(methacrylic acid-co-acrylamide) polymer hydrogel was synthesized by a free radical mechanism in methylene bisacrylamide as a crosslinker and potassium persulfate as an initiator. Bentonite, montmorillonite, and Cloisite 30B biodegradable clay nanoparticles were added to improve hydrogel mechanical properties and swelling speed. Fourier-transform infrared spectroscopy, X-ray diffraction (XRD), scanning electron microscopy, and thermogravimetric analysis (TGA) were used to check the structural properties. XRD analysis and TGA evaluated the mechanical properties and thermal stability. Also, it was determined from the scanning electron microscope that at the nanoscale, the distribution of clay nanoparticles among the hydrogel links was regular, and no accumulation was seen among the molecules, which indicates the continuous structure of nanocomposite hydrogels. On the other hand, TGA analysis proved the thermal stability of nanocomposites after adding clay nanoparticles. Also, the swelling rate of co-polymer and nanocomposite hydrogels was obtained by measuring the swelling rate. The desired results increased, higher than the swelling rate attributed to poly(methacrylic acid-acrylamide)/Cloisite 30B nanocomposite hydrogel. The results show that they are successful in addition to nanoparticles and increase the swelling speed of hydrogels. The analyses also show improved mechanical properties, increased surface strength and thermal stability, and optimal distribution of nanoparticles on the surface of hydrogels. The addition of clay nanoparticles to the performance of the co-polymer hydrogel increased the swelling rate up to 15 times, which can be used in the adsorption, drug delivery, and polymerization industries.

Keywords: Hydrogel; Swelling; Free radical polymerization; Nanoclay; Nanocomposite

1. Introduction

Today, the use of polymeric materials in various industries is very important. One of the most important polymers is hydrogels, which have many applications in various fields. In general, hydrogels are divided into natural and synthetic categories. Natural hydrogels are extracted from raw organic materials such as carboxymethyl cellulose and

alginate, primarily biodegradable. Hydrogels from laboratory chemicals are synthesized in chemical and polymer laboratories, such as gelatins [1–3]. Also, hydrogels are divided into two groups in terms of binding: co-polymers and biopolymers, which are often the basis of co-polymers and monomers. The basis of biopolymers is a captured biopolymer [4,5]. Co-polymer hydrogels have a high adsorption rate due to effective networking. Still, the most critical

* Corresponding author.

issue regarding adsorption by hydrogels is the increase in adsorption rate and swelling of these hydrogels [6,7]. One of the active and functional monomers in co-polymer bonds is methacrylic acid, which has an effective bond due to its acidic structure and high activity coefficient. The water solubility of alkyl methacrylate's is higher than that of insoluble components.

Some functional esters have excellent solubility in water or hydrolysis. Methacrylic acid and its common esters are soluble in most organic solvents, so it can play an essential role in the discussion of swelling [5–7]. Another effective monomer in co-polymer bonding is acrylamide, which has high bonding strength. It is a white, solid, odorless crystalline substance that dissolves in water, ethanol, ether, and chloroform. Acrylamide decomposes into preacids, bases, oxidizing agents, and iron salts. Decomposes without heating into ammonia and decomposes on heating to carbon monoxide, carbon dioxide, and nitrogen oxides. Acrylamide can be prepared by hydrolysis of acrylonitrile with nitrile hydrate. Polyacrylamide is one of the cleaning agents used to facilitate the purification of drinking water and the removal of waste products. Polyacrylamide is also used to manufacture adhesives, paper, plastics, and cosmetics [8,9]. Also, some hydrogels can decompose due to high heat and pressure during adsorption. Today, some nanoparticles, such as activated carbon, clay, industrial nanoparticles, etc., are used to improve the performance and efficiency of hydrogels [7,9]. Different nanoparticles have different efficiencies and functions. This efficiency depends on the inflation rate, the increase in research efficiency, and the final research costs. In the discussion of hydrogels, increasing the inflation rate is one of the most critical issues in selecting the appropriate nanoparticles [9,10]. Today, hydrogels are used in the field of pollutant adsorption [11], drug delivery [12], bioengineering [13], medicine [14], and agriculture [15], which has made significant progress in these areas. Different nanoparticles are used to strengthen hydrogel bonds. The most common nanoparticles used in hydrogels are chitosan-based nanoparticles [10], alginate [11], metals such as silver [12], and clay. Clay nanoparticles are suitable for improving hydrogels' performance and mechanical properties due to their availability, cheapness, high thermal resistance, formation of regular octagonal networks, and biodegradability [16,17]. By reinforcing them and increasing the swelling rate of these hydrogels, clay nanoparticles form bonds in the co-polymer networks of hydrogels, thus increasing the volume and adsorption capacity. Types of clay nanoparticles, such as natural and modified montmorillonites such as Cloisite 30B, bentonite, kaolin, etc., are

available [18–20]. These nanoparticles have a stable structure due to their octagonal structure and silicate bonds, which increases the number of effective bonds between these nanoparticles and the structure of co-polymer hydrogels [21]. Also, because these nanoparticles are extracted from the environment, they are readily biodegradable and recyclable [22]. Increasing the swelling of these hydrogels with the help of clay nanoparticles can be used to adsorb colored pollutants, heavy metal pollutants, oil cuts, and other pollutants floating in surface water [23]. Increased inflation can also be studied and used in polymer studies such as drug delivery [24] and intelligent polymers [25], and agriculture [26].

Hydrogels have attracted the attention of researchers in various research fields. Hydrogels are a challenge for researchers to synthesize hydrogels by different methods, such as self-made gel, conducting hydrogels, free radicals, or hydrogels reinforced with ionic conductors. Comparing the properties and improving the performance of hydrogels in different ways has provided the basis for advancing various sciences involved with these hydrogels. For example, the synthesis of conductive hydrogels based on two-dimensional (2D) nanomaterials has made significant progress in coating sensors. Or in the field of sensors, ionic conductive hydrogels are used as skin sensors [27,28].

Among other parts of using hydrogels, we can mention the construction of supercapacitors in the conduction field. Hydrogels can enhance supercapacitors' properties, such as conduction, corrosion, and flexibility. One of the most important and common uses of hydrogels is the removal of dyes and heavy metals soluble in water. He mentioned nanocomposite hydrogels for adsorbing pollutants such as methylene blue, malachite green, rhodamine B, and iron, calcium, and chromium ions. Strengthening many parts of the structure of hydrogels, such as swelling, high conductivity, self-adhesion, and antifreeze ability, poses different challenges for researchers to provide maximum efficiency of hydrogels. [29,30].

The swelling rate of nanocomposite hydrogels is very important because as the hydrogel swells, the number of active sites increases, and it prepares for different reactions. A hydrogel must have a high swelling rate and maintain its structure [13,14].

This study synthesized polymethacrylic acid co-polymer hydrogels with acrylamide by a free radical mechanism and added montmorillonite, bentonite, and Cloisite 30B clay nanoparticles (Fig. 1) to improve mechanical performance and increase adsorption and swelling. Fourier-transform infrared spectroscopy (FTIR), scanning electron

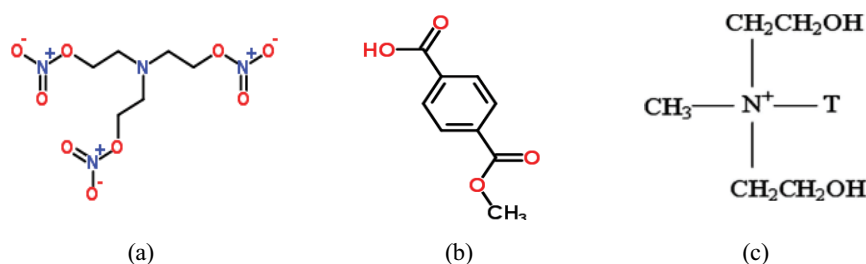


Fig. 1. Nanoparticles structure, (a) bentonite, (b) montmorillonite, and (c) Cloisite 30B.

microscopy (SEM), energy-dispersive X-ray spectroscopy (EDX), dot mapping, thermogravimetric analysis (TGA), and X-ray diffraction (XRD) analysis were used to improve the properties of nanocomposites. Also, to evaluate the swelling of co-polymer hydrogels and nanocomposite hydrogels, swelling tests were performed in 5%, 10%, and 15% by weight of clay nanoparticles, and the effect of increasing nanoparticles on the hydrogels was investigated.

2. Materials and methods

Methacrylic acid (MAA) (MW: 86.06 g/L) and acrylamide (AAM) (MW: 71.08 g/L) were purchased from (Merck, Germany). *N,N'*-methylene bisacrylamide (MBA) cross-linker (MW: 154.17 g/L) was also prepared from (Merck, Germany). Potassium persulfate (KPS) was provided by (Samchon, Korea); Cloisite 30B (Southern Clay, USA) was obtained; bentonite was purchased from (Sigma-Aldrich, Munich, Germany); and montmorillonite was obtained from (Southern Clay Company, USA) and used without any pretreatments.

2.1. Preparation of nanocomposite hydrogels

For the preparation of poly(methacrylic acid-co-acrylamide) hydrogel, poly(MMA-co-AAm)/bentonite, poly(MMA-co-AAm)/MMT, and poly(MMA-co-AAm)/Cloisite 30B nanocomposite hydrogels, the free radical polymerization method was used. This method neutralized MAA (5 g) with NaOH solution (8 mol/L) for future use. Neutral methacrylic acid was poured into a nozzle with a mechanical stirrer, nitrogen gas inlet, and water flow to regulate Debby and the thermometer. Specific amounts of clay nanoparticles (0%–15% by weight) were dispersed in 2 g of acrylamide and 0.02 g of methylene bis-acrylamide as a cross-linker and 10 mL of ionized water ultrasonic prep device. This process was performed at 25°C for 30 min to disperse the nanoclays in acrylamide solution. After complete sonication, the solution was added to a three-necked flask containing methacrylic acid. During the synthesis process, nitrogen gas was blown continuously to fill the medium and completely remove the oxygen molecules from the synthesis medium. After mixing at 70°C, potassium persulfate (KPS) was added to the flask as a primer to generate free radicals. After 20–30 min of mixing the synthesizing materials, a gel was formed. The heating was stopped, and the gels were rested for 3–4 h to complete the polymerization process. To remove non-reactive monomers, the hydrogels were washed several times with deionized water. The synthesized hydrogels were dried at 55°C for 48 h in an oven. The dried hydrogels were then crushed in 250–500 μm to be carefully tested at regular sizes and stored for further use. Poly(methacrylic acid-co-acrylamide) hydrogels, without nanoparticles, were synthesized according to the above method for comparison. Fig. 2 shows the flowchart of nanocomposite preparation.

2.2. Investigation of swelling behavior of hydrogels

An inflation test was performed to evaluate and compare the swelling behavior of co-polymer hydrogels and

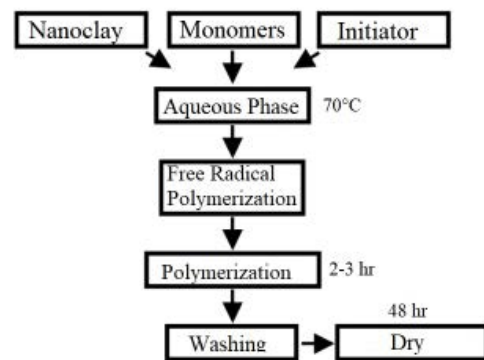


Fig. 2. Flowchart for preparation of nanocomposite hydrogel.

nanocomposite hydrogels. For this purpose, 10 g of hydrogel was poured into 300 mL of deionized water and rested at the same temperature for 48 h. The swollen hydrogels suspended in water were then centrifuged to completely separate from the aqueous phase. The hydrogels were weighed after separation from ionized distilled water, then the swelling rate of each was calculated by Eq. (1) and compared with each other. With this method, besides investigating the effect of adding clay nanoparticles on the swelling rate of co-polymer hydrogels, the swelling effectiveness of bentonite, montmorillonite, and Cloisite 30B clay nanoparticles was also investigated compared [31–34].

$$\text{Swelling} = \frac{W_{\text{wet}} - W_{\text{Dry}}}{W_{\text{Dry}}} \quad (1)$$

where W_{wet} and W_{Dry} are the weight of wet and dry hydrogel samples, respectively. Fig. 3 shows the steps for performing an inflation test.

2.3. Method of characterization

From FTIR, SEM, XRD, and TGA analysis to study the structure and mechanical properties of poly(MMA-co-AAm) co-polymer hydrogel and poly(MMA-co-AAm)/bentonite, poly(MMA-co-AAm)/MMT, and poly(MMA-co-AAm)/Cloisite 30B nanocomposite hydrogels were used. The device (Tensor 27, Bruker, Germany) was used to investigate the Fourier-transform X-ray spectroscopy. Materials were scanned for extended analysis at 400–4,000 cm^{-1} . Field-emission scanning electron microscopy (FE-SEM MIRA3, FEG-SEM, TUSCAN, Czech Republic) was used to study the surface morphology of hydrogels. This device is equipped with X-ray scattering (EDX) analysis. The samples were coated with gold-plated spray steam. The main samples' thickness profiles were obtained using EDX and dot-mapping (Microanalysis Oxford Instruments Model 7718 INCA PentaFET) to determine nanoclays' distribution on nanocomposite hydrogels' surface. X-ray diffraction measure (Siemens S5000, Germany) was used to analyze XRD, X-ray diffraction patterns equipped with a CuK α radiation source with a scan speed of 0.2°/min at ambient temperature and a 40 kV and a current of 30 mA. The Bragg equation ($n\lambda = 2d \sin\theta$) with $\lambda = 4.15418 \text{ nm}$ was used to calculate the silicate

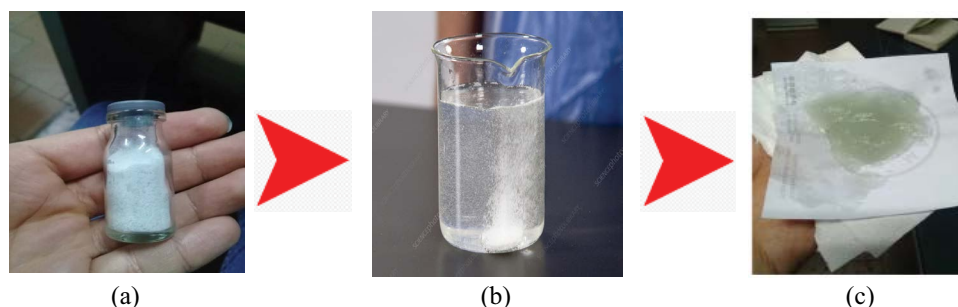


Fig. 3. Swelling test steps of poly(methacrylic acid-co-acrylamide)/Cloisite 30B hydrogel samples. (a) Powdered hydrogel, (b) mixing hydrogel and distilled water and (c) swollen hydrogel.

layer's base distance (d001). Also, this analysis was performed in the range of diffraction angle (2θ) between 2° to 25° . The thermal stability of the samples was analyzed by Thermography analysis by the analyzer (Linseis N81 A1750, USA) at a heating rate of $10^\circ\text{C}/\text{min}$ and in the temperature range of 25°C – 900°C in a nitrogen atmosphere. Also, swelling test tests were used in the same environment for all samples to test the effect of the contact time of the hydrogel with the aqueous medium and change the swelling rate.

3. Results and discussion

FTIR, SEM, EDX, Map, TGA, and XRD analysis were used to investigate nanocomposites' properties. Also, the swelling rate of nanocomposites in different amounts of clay nanoparticles was discussed, and the results of each will be examined.

3.1. Investigation of FTIR analysis

To study the structure of poly(MMA-co-AAm) co-polymer hydrogel and poly(MMA-co-AAm)/bentonite, poly(MMA-co-AAm)/MMT, and poly(MMA-co-AAm)/Cloisite 30B nanocomposite hydrogels from FTIR analysis was used. Fig. 4 shows the spectroscopic results of hydrogel samples. As can be seen in Fig. 4a for poly(MMA-co-AAm) co-polymer hydrogels, there are several peaks and vibration intervals, with the peak at wavenumber $1,751.29\text{ cm}^{-1}$ corresponding to the $-\text{COOH}$ group tensile, which is formed from the reaction of methacrylic acid and acrylamide monomers, which confirms the existence of a co-polymer bond between the monomers in the hydrogel [35]. The $1,651\text{ cm}^{-1}$ wavenumber peak corresponds to the $\text{C}=\text{C}$ group [36]. However, the intensity of the peaks decreases significantly, and the wavenumbers are slightly distorted, which may be attributed to the molecular bonding between the monomers and the formation of a co-polymer bond. Also, the peak in the wavenumber of $3,429.29\text{ cm}^{-1}$ is related to the tension of the hydrogen–nitrogen bond in the acrylamide structure. The diagrams in Fig. 4b–d show the graphs of the broad spectrum of poly(MMA-co-AAm)/bentonite, poly(MMA-co-AAm)/MMT, and poly(MMA-co-AAm)/Cloisite 30B nanocomposite hydrogels. In general, as shown in the diagrams, the number of vibrations has decreased compared to the co-polymer hydrogel diagram. At the same time, the wavenumbers have been slightly wider and longer,

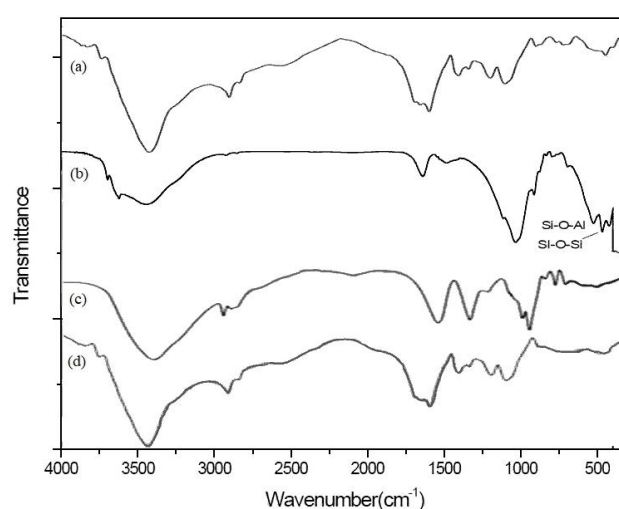


Fig. 4. Fourier-transform infrared spectra of (a) poly(MMA-co-AAm) co-polymer hydrogel, (b) poly(MMA-co-AAm)/bentonite, (c) poly(MMA-co-AAm)/MMT, and (d) poly(MMA-co-AAm)/Cloisite 30B nanocomposite hydrogels.

indicating the favorable effect of adding clay particles on the hydrogel swelling [37]; in the results of the diagrams of nanocomposite hydrogels (Fig. 4), the swelling of the wavenumber intervals of the samples increases. Vibrations in the range $1,600$ – $1,700\text{ cm}^{-1}$ are related to the co-polymer bonds between MAA and AAm. Peaks in the structure of nanocomposites in the range of 400 – 500 cm^{-1} are associated with the tensile strength of Si-O-Si and Si-O-Al . Also, the vibrations in the diagram in the ranges above $2,000\text{ cm}^{-1}$ are related to carbon and C-H hydrogel bonds. The results of FTIR analysis show that the pores of nanocomposite hydrogels are widened for further swelling [38].

3.2. XRD analysis

The results of XRD analysis are shown in Figs. 5 and 6. Fig. 5 shows the analysis results of bentonite, montmorillonite, and Cloisite 30B nanoparticles. Also, Fig. 6 shows the results of the analysis of poly(MMA-co-AAm) co-polymer, poly(MMA-co-AAm)/bentonite, poly(MMA-co-AAm)/MMT, and poly(MMA-co-AAm)/Cloisite 30B nanocomposite hydrogels. Fig. 3a relates to the bentonite diagram.

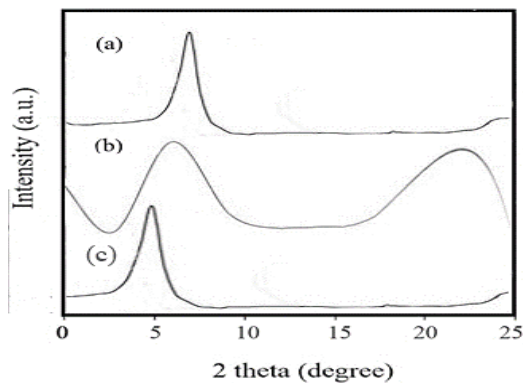


Fig. 5. X-ray diffraction patterns of (a) bentonite, (b) MMT and (c) Cloisite 30B.

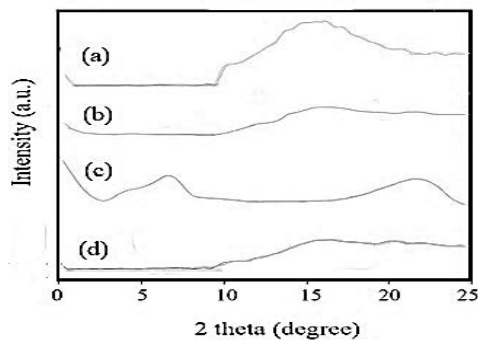


Fig. 6. X-ray diffraction patterns of (a) poly(MMA-co-AAm), (b) poly(MMA-co-AAm)/bentonite, (c) poly(MMA-co-AAm)/MMT, and (d) poly(MMA-co-AAm)/Cloisite 30B.

The peak observed in the range of $2\theta = 5^\circ\text{--}10^\circ$ (specified at $2\theta = 5.7^\circ$) corresponds to the base distance (d_{001}) for the bentonite nanoclay layer structure. In Fig. 5b of the montmorillonite diagram, the peaks observed at $2\theta = 6.92^\circ$ and $2\theta = 23.18^\circ$ are related to the layered and octagonal structure of the montmorillonite nanoparticles, respectively [39,40]. Also, Fig. 5c is related to the Cloisite 30B nanoparticle diagram, from which the peak $2\theta = 4.53^\circ$ can be seen, associated with the nanoparticle layer structure [41]. Also, by examining Fig. 6a related to XRD polymer co-polymer hydrogel poly(MMA-co-AAm) and comparing it with the results of poly(MMA-co-AAm)/bentonite, poly(MMA-co-AAm)/MMT, and poly(MMA-co-AAm)/Cloisite 30B nanocomposite hydrogels. As shown in Fig. 6b–d, nanocomposite hydrogels' structure means that by adding clay nanoparticles, the structure of the hydrogels becomes layered and cohesive, increasing the strength of the swelling [42].

3.3. Thermogravimetric analysis

Fig. 7 shows the TGA thermometric analysis results to evaluate the samples' thermal stability. The results of the TGA analysis showed that weight loss of co-polymer and nanocomposite hydrogel samples was performed in three stages. The first stage of weight loss occurred at $50^\circ\text{C--}150^\circ\text{C}$, possibly due to the water content's evaporation in the

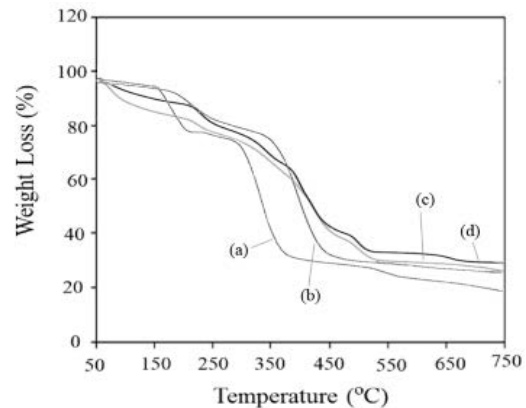


Fig. 7. Thermogravimetric analysis of (a) poly(MMA-co-AAm), (b) poly(MMA-co-AAm)/bentonite, (c) poly(MMA-co-AAm)/MMT, and (d) poly(MMA-co-AAm)/Cloisite 30B.

samples. At this stage, the weight loss of nanocomposite samples is more than the co-polymer hydrogel sample, which is due to more water molecules in the structure of nanocomposite hydrogels. The second stage of weight loss was performed in the temperature range of $200^\circ\text{C--}450^\circ\text{C}$, where the hydrogels lost a significant part of their weight, which could be related to the destruction of acrylamide bonds and the breakdown of monomer bonds. Also, the C–H bond of methacrylic acid, which is the predominant monomer of the hydrogel, decomposes at this stage. The final weight loss can be due to the decomposition and destruction of the structure of the mentioned materials, at which stage we see a slight weight loss [41,43]. As shown in Fig. 7, adding bentonite, montmorillonite, and Cloisite 30B nanoparticles increases the thermal stability of nanocomposite hydrogels. In addition, the comparison of the samples shows that adding nanoclay to the co-polymer hydrogel significantly increased the thermal stability of the nanocomposites during the heating steps. This result may be due to the layered structure of the nanoparticles. The strong interaction of hydrogen bonds with methacrylic acid and acrylamide monomers evaporates water molecules, breaks chains, and opens nanocomposite layers, increasing nanocomposites' swelling rate [44].

3.4. Scanning electron microscopy and energy-dispersive X-ray spectroscopy

Surface morphology analysis by SEM was used to study the surface changes and morphology of co-polymer and nanocomposite samples. According to the results of SEM analysis in Fig. 8, micrographs of co-polymer hydrogel samples and its comparison with nanocomposite samples, due to capillary forces, water is adsorbed through the pores between the hydrogels, and the higher the swelling, the larger the pores. Swelling in hydrogels depends on the size and distance between the particles. The shapes of nanocomposite hydrogel samples show the opening of pores and layers and increased swelling power [45]. Fig. 9 shows the point mapping results of nanocomposite hydrogels with Si distribution as markers. Excellent and regular dispersion

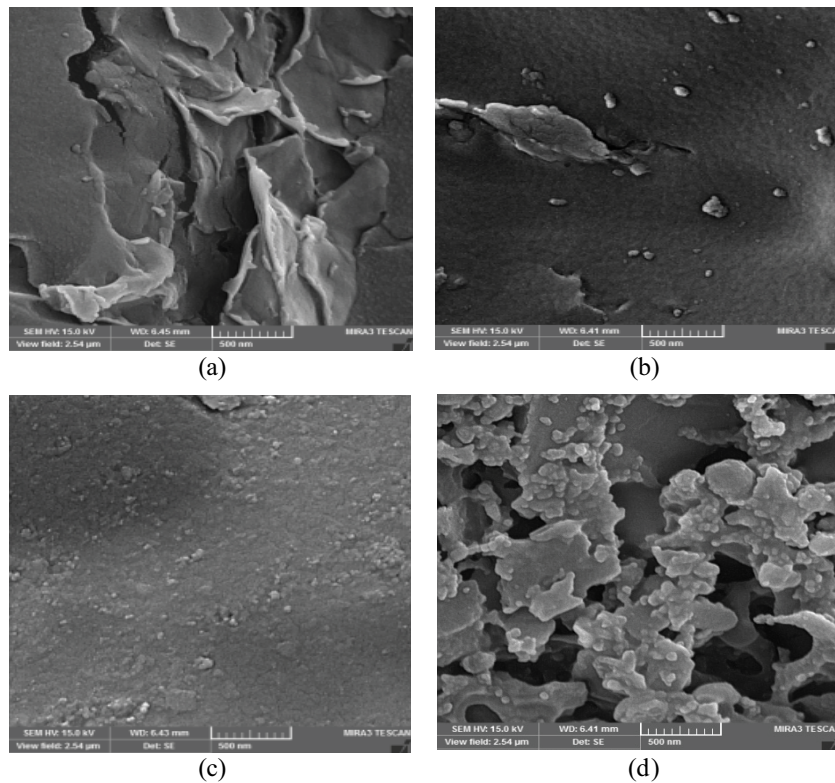


Fig. 8. Scanning electron microscopy for (a) poly(MMA-co-AAm), (b) poly(MMA-co-AAm)/bentonite, (c) poly(MMA-co-AAm)/MMT, and (d) poly(MMA-co-AAm)/Cloisite 30B (SEM HV: 15 kV, view field: 2.54 μm , and SEM Mag: 50.0 kx).



Fig. 9. Dot mapping image of poly(MAA-co-AAm)/10 wt.% MMT (accelerating voltage (kV): 15.0), crystal: Si, and magnification: 2,500).

and no accumulation of nanoparticles can be observed in the hydrogel matrix. After adsorbing water and swollen pores and surface roughness, the hydrogels are almost saturated due to the penetration of water molecules in the pores [46]. Also, stable dispersion of Cloisite 30B nanoparticles compared to other nanoparticles shows a favorable effect compared to other cases. The SEM analysis also found that the distribution of clay nanoparticles in the matrix of

Table 1

Swelling test results of the co-polymer and nanocomposite hydrogel samples with different percentages of nanoparticles

Nanoclay (wt.%) hydrogel	0	5	10	15
Poly(MMA-co-AAm)	273.5	–	–	–
Poly(MMA-co-AAm)/bentonite	–	1,200	2,500	2,100
Poly(MMA-co-AAm)/MMT	–	1,900	2,850	2,300
Poly(MMA-co-AAm)/Cloisite 30B	–	2,400	3,500	3,000

co-polymer bonds was regular, proving that the number of active matrices of nanocomposite hydrogels has increased and increased the strength and efficiency of the hydrogel. This study shows that the presence of nanoparticles has increased the efficiency of hydrogels (for example, in the field of water-soluble pollutant adsorption, it increases the amount of adsorption).

3.5. Effect of different types of clay nanoparticles on swelling

The inflation rate of the studied samples was examined. The results are presented in Table 1 and Fig. 10. Examples include poly(MMA-co-AAm) co-polymer hydrogel without the addition of nanoparticles and compare it with the results of poly(MMA-co-AAm)/bentonite, poly(MMA-co-AAm)/MMT, and poly(MMA-co-AAm)/Cloisite 30B nanocomposite hydrogels with 5%, 10%, and 15% by weight. As it is clear from the results, the addition of bentonite, MMT & Cloisite

Table 2

Comparison of swelling of poly(MAA-co-AAm) hydrogel and nanocomposites hydrogel with other hydrogels in swelling rate

Hydrogel	Swelling (%)	Application	References
Dextran/nanocrystalline β -tricalcium phosphate	530	Medical	[48]
Poly(acrylamide-co-itaconic acid)/MWCNT	460	Adsorption	[49]
Oxidized starch/ZnO	1,260	Medical	[32]
CMC/polyvinylpyrrolidone/silica	890	Agriculture	[50]
Starch-g-poly(AA-co-AAm)/polyvinyl alcohol/clino	370	Hygiene products	[51]
N-isopropylacrylamide/MMT	550	Drug delivery	[52]
Poly(N-isopropylacrylamide)	1,600	Adsorption	[53]
Poly(acrylamide-co-itaconic acid)-hydroxyapatite	1,800	Swelling	[54]
Starch-g-poly(4-acrylamidobenzoic acid)/polycaprolactone 10	2,600	Drug delivery	[15]
Chitosan/MMT-poly(2-acrylamido-2-methylpropane sulfonic acid)	700	Medical & drug delivery	[16]
Poly(MAA-co-AAm)	273.5	Adsorption, medical & drug delivery	This work
Poly(MAA-co-AAm)/bentonite	2,500	Adsorption, medical & drug delivery	This work
Poly(MAA-co-AAm)/MMT	2,850	Adsorption, medical & drug delivery	This work
Poly(MAA-co-AAm)/Cloisite 30B	3,500	Adsorption, medical & drug delivery	This work

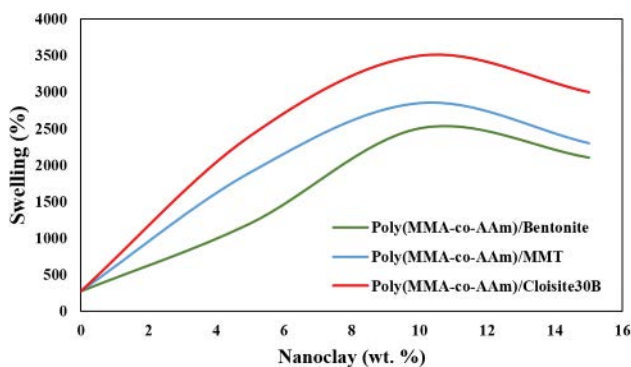


Fig. 10. Swelling test results of co-polymer and nanocomposite hydrogel samples with different percentages of nanoparticles.

30B-type clay nanoparticles has significantly improved the swelling rate of hydrogel samples. In addition, by comparing the swelling of hydrogels, we observe that with increasing the weight percentage of the samples, the swelling rate increases, but after 10% by weight, due to the saturation of the active sites of the hydrogels and bonding with nanoparticles, the swelling rate decreases [47]. Also, the effectiveness of Cloisite 30B clay nanoparticles is higher than bentonite and MMT. Table 2 also compares inflation test results with similar studies of other hydrogels. A high swelling rate is critical, along with maintaining the structure of the hydrogel. Comparing the research results with similar results of other studies, it is clear that the swelling rate of the nanocomposite hydrogels studied is very high. Also, from the SEM results, it is clear that the structure of the hydrogels is maintained. On the other hand, investigating the swelling rate of hydrogels shows an increase in the strength of

hydrogels and the stability of water retention in the active matrices of hydrogels after adding clay nanoparticles.

4. Conclusion

Structural characterization was performed by FTIR, XRD, SEM, EDX, and TGA techniques. The XRD analysis found that the peaks in the region of $2\theta = 5$ nanoparticles were destroyed after the formation of the hydrogel, which indicates the opening of the hydrogel layers. FTIR analysis showed that adding clay nanoparticles did not change the main structure of the hydrogel. Still, as the wavelengths of the nanocomposites widened, it was found that the acceptance capacity of the active sites increased. Also, XRD analysis found that the initial peaks of the co-polymer hydrogel are widely reduced by adding clay nanoparticles, which indicates structural cohesion. SEM results showed that adding clay nanoparticles expands the structure of hydrogels and increases the number of active sites. TGA analysis showed that adding clay nanoparticles significantly increased the hydrogels' thermal stability so that the co-polymer hydrogel's weight loss was reduced by adding nanoparticles from 90% by weight to about 83%. To conclude, by examining the swelling rate of co-polymer and nanocomposite hydrogels, it was found that adding clay nanoparticles significantly increases the swelling rate of the hydrogel and poly(MMA-co-AAm)/Cloisite 30B nanocomposite hydrogel by 10% by weight. It had the highest inflation. Cloisite 30B type clay nanoparticles showed the most significant effect on swelling, 3,500% in poly(MAA-co-AAm)/10% Cloisite 30B hydrogel. From the results obtained by comparing the studied hydrogels with similar works, it is clear that the synthesized nanocomposite hydrogels have a significant advantage in high swelling rate and structural strength, making this study

successful. The hydrogels synthesized in this study can be used in the adsorption of pollutants and drug delivery. Also, due to the biodegradability of hydrogel ingredients, it can be used on a large scale in the environment.

References

- [1] Y. Li, X. Hou, Y. Pan, L. Wang, H. Xiao, Redox-responsive carboxymethyl cellulose hydrogel for adsorption and controlled release of dye, *Eur. Polym. J.*, 123 (2020) 109447, doi: 10.1016/j.eurpolymj.2019.109447.
- [2] C.F. Mok, Y.C. Ching, F. Muhamad, N.A. Abu Osman, N.D. Hai, C.R.C. Hassan, Adsorption of dyes using poly(vinyl alcohol) (PVA) and PVA-based polymer composite adsorbents: a review, *J. Polym. Environ.*, 28 (2020) 775–793.
- [3] C.B. Godiya, S. Kumar, Y. Xiao, Amine functionalized egg albumin hydrogel with enhanced adsorption potential for diclofenac sodium in water, *J. Hazard. Mater.*, 393 (2020) 122417, doi: 10.1016/j.jhazmat.2020.122417.
- [4] C. Bai, L. Wang, Z. Zhu, Adsorption of Cr(III) and Pb(II) by graphene oxide/alginate hydrogel membrane: characterization, adsorption kinetics, isotherm and thermodynamics studies, *Int. J. Biol. Macromol.*, 147 (2020) 898–910.
- [5] S.J. Peighambaroust, E. Ghergherehchi, P. Mohammadzadeh Pakdel, H. Aghdasinia, Facile removal of methylene blue using carboxymethyl cellulose grafted polyacrylamide/carbon black nanocomposite hydrogel, *J. Polym. Environ.*, 31 (2022) 939–953.
- [6] L. Chen, Y. Zhu, Y. Cui, R. Dai, Z. Shan, H. Chen, Fabrication of starch-based high-performance adsorptive hydrogels using a novel effective pretreatment and adsorption for cationic methylene blue dye: behavior and mechanism, *Chem. Eng. J.*, 405 (2021) 126953, doi: 10.1016/j.cej.2020.126953.
- [7] M.A.H. Badsha, M. Khan, B. Wu, A. Kumar, I.M.C. Lo, Role of surface functional groups of hydrogels in metal adsorption: from performance to mechanism, *J. Hazard. Mater.*, 408 (2021) 124463, doi: 10.1016/j.jhazmat.2020.124463.
- [8] W. Lu, Z. Dai, L. Le, J. Liu, S. Wang, H. Yang, C. Cao, L. Liu, T. Chen, B. Zhu, L. Sun, L. Chen, H. Li, P. Zhang, Preparation of composite hydrogel (PCG) and its adsorption performance for uranium(VI), *J. Mol. Liq.*, 303 (2020) 112604, doi: 10.1016/j.molliq.2020.112604.
- [9] H. Safarzadeh, S.J. Peighambaroust, S.H. Peighambaroust, Application of a novel sodium alginate-graft-poly(methacrylic acid-co-acrylamide)/montmorillonite nanocomposite hydrogel for removal of malachite green from wastewater, *J. Polym. Res.*, 30 (2023) 157, doi: 10.1007/s10965-023-03531-x.
- [10] R.R. Palem, K.M. Rao, G. Shimoga, R.G. Saratale, S.K. Shinde, G.S. Ghodake, S.H. Lee, Physicochemical characterization, drug release, and biocompatibility evaluation of carboxymethyl cellulose-based hydrogels reinforced with sepiolite nanoclay, *Int. J. Biol. Macromol.*, 178 (2021) 464–476.
- [11] M.T. Nakhjiri, G.B. Marandi, M. Kurdtabar, Preparation of magnetic double network nanocomposite hydrogel for adsorption of phenol and p-nitrophenol from aqueous solution, *J. Environ. Chem. Eng.*, 9 (2021) 105039, doi: 10.1016/j.jece.2021.105039.
- [12] Y. Cao, Y. Cheng, G. Zhao, Near-infrared light-, magneto-, and pH-responsive GO-Fe₃O₄/poly(*N*-isopropylacrylamide)/alginate nanocomposite hydrogel microcapsules for controlled drug release, *Langmuir*, 37 (2021) 5522–5530.
- [13] X. Zhai, C. Ruan, J. Shen, C. Zheng, X. Zhao, H. Pan, W.W. Lu, Clay-based nanocomposite hydrogel with attractive mechanical properties and sustained bioactive ion release for bone defect repair, *J. Mater. Chem. B*, 9 (2021) 2394–2406.
- [14] S. Nazir, M.U. Aslam Khan, W.S. Al-Arjan, S.I. Abd Razak, A. Javad, M.R. Abdul Kadir, Nanocomposite hydrogels for melanoma skin cancer care and treatment: *in-vitro* drug delivery, drug release kinetics and anti-cancer activities, *Arabian J. Chem.*, 14 (2021) 103120, doi: 10.1016/j.arabjc.2021.103120.
- [15] D. Das, P. Prakash, P.K. Rout, S. Bhaladhare, Synthesis and characterization of superabsorbent cellulose-based hydrogel for agriculture application, *Starch-Starke*, 73 (2021) 1900284, doi: 10.1002/star.201900284.
- [16] H. Chen, T. Liu, Y. Meng, J. Lu, H. Wang, Novel graphene oxide/aminated lignin aerogels for enhanced adsorption of malachite green in wastewater, *Colloids Surf., A*, 603 (2020) 125281, doi: 10.1016/j.colsurfa.2020.125281.
- [17] H. Al-Aidy, E. Amdeha, Green adsorbents based on polyacrylic acid-acrylamide grafted starch hydrogels: the new approach for enhanced adsorption of malachite green dye from aqueous solution, *Int. J. Environ. Anal. Chem.*, 101 (2021) 2796–2816.
- [18] H. Mittal, A. Al Alili, S.M. Alhassan, High efficiency removal of methylene blue dye using κ -carrageenan-poly(acrylamide-co-methacrylic acid)/AQSOA-Z05 zeolite hydrogel composites, *Cellulose*, 27 (2020) 8269–8285.
- [19] O. Duman, T.G. Polat, C.O. Diker, S. Tunc, Agar/ κ -carrageenan composite hydrogel adsorbent for the removal of methylene blue from water, *Int. J. Biol. Macromol.*, 160 (2020) 823–835.
- [20] S. Nayak, S.R. Prasad, D. Mandal, P. Das, Carbon dot cross-linked polyvinylpyrrolidone hybrid hydrogel for simultaneous dye adsorption, photodegradation and bacterial elimination from waste water, *J. Hazard. Mater.*, 392 (2020) 122287, doi: 10.1016/j.jhazmat.2020.122287.
- [21] L. Jiang, Y. Wen, Z. Zhu, C. Su, S. Ye, J. Wang, X. Liu, W. Shao, Construction of an efficient nonleaching graphene nanocomposites with enhanced contact antibacterial performance, *Chem. Eng. J.*, 382 (2020) 122906, doi: 10.1016/j.cej.2019.122906.
- [22] S. Manna, P. Das, P. Basak, A.K. Sharma, V.K. Singh, R.K. Patel, J.K. Pandey, V. Ashokkumar, A. Pugazhndhi, Separation of pollutants from aqueous solution using nanoclay and its nanocomposites: a review, *Chemosphere*, 280 (2021) 130961, doi: 10.1016/j.chemosphere.2021.130961.
- [23] A. Verma, S. Thakur, G. Mamba, P. Teek, R.K. Gupta, P. Thakur, V.K. Thakur, Graphite modified sodium alginate hydrogel composite for efficient removal of malachite green dye, *Int. J. Biol. Macromol.*, 148 (2020) 1130–1139.
- [24] G.P. Rajalekshmy, M.R. Rekha, Strontium ion cross-linked alginate-g-poly(PEGMA) xerogels for wound healing applications: *in-vitro* studies, *Carbohydr. Polym.*, 251 (2021) 117119, doi: 10.1016/j.carbpol.2020.117119.
- [25] E.-R. Kenawy, M.M. Azaam, E.M. El-nshar, Sodium alginate-g-poly(acrylic acid-co-2-hydroxyethyl methacrylate)/montmorillonite superabsorbent composite: preparation, swelling investigation and its application as a slow-release fertilizer, *Arabian J. Chem.*, 12 (2019) 847–856.
- [26] M. Shahbazi, H. Jäger, S.J. Ahmadi, M. Lacroix, Electron beam crosslinking of alginate/nanoclay ink to improve functional properties of 3D printed hydrogel for removing heavy metal ions, *Carbohydr. Polym.*, 240 (2020) 116211, doi: 10.1016/j.carbpol.2020.116211.
- [27] X. Wang, N. Li, J. Yin, X. Wang, L. Xu, T. Jiao, Z. Qin, Interface interaction-mediated design of tough and conductive MXene-composited polymer hydrogel with high stretchability and low hysteresis for high-performance multiple sensing, *Sci. China Mater.*, 66 (2023) 272–283.
- [28] Z. Qin, S. Liu, J. Bai, J. Yin, N. Li, T. Jiao, Ionic conductive hydroxypropyl methyl cellulose reinforced hydrogels with extreme stretchability, self-adhesion and anti-freezing ability for highly sensitive skin-like sensors, *Int. J. Biol. Macromol.*, 220 (2022) 90–96.
- [29] J. Yin, K. Wei, J. Zhang, S. Liu, X. Wang, X. Wang, Q. Zhang, Z. Qin, T. Jiao, MXene-based film electrode and all-round hydrogel electrolyte for flexible all-solid supercapacitor with extremely low working temperature, *Cell Rep. Phys. Sci.*, 3 (2022) 100893, doi: 10.1016/j.xcrp.2022.100893.
- [30] Z. Liu, N. Li, P. Liu, Z. Qin, T. Jiao, Highly sensitive detection of iron ions in aqueous solutions using fluorescent chitosan nanoparticles functionalized by Rhodamine B, *ACS Omega*, 7 (2022) 5570–5577.
- [31] H. Khatooni, S.J. Peighambaroust, R. Foroutan, R. Mohammadi, B. Ramavandi, Facile removal of methylene blue using carboxymethyl cellulose grafted polyacrylamide/carbon

- black nanocomposite hydrogel, *J. Polym. Environ.*, 31 (2023) 297–311.
- [32] H. Namazi, M. Hasani, M. Yadollahi, Antibacterial oxidized starch/ZnO nanocomposite hydrogel: synthesis and evaluation of its swelling behaviours in various pHs and salt solutions, *Int. J. Biol. Macromol.*, 126 (2019) 578–584.
- [33] S. Mohammadi, M. Vafaie Sefti, M. Baghban Salehi, A. Mousavi Moghadam, S. Rajaei, H. Naderi, Hydrogel swelling properties: comparison between conventional and nanocomposite hydrogels for water shutoff treatment, *Asia-Pac. J. Chem. Eng.*, 10 (2015) 743–753.
- [34] H. Safarzadeh, S.J. Peighambardoust, S.H. Mousavi, R. Mohammadi, S.H. Peighambardoust, Adsorption of methyl violet dye from wastewater using poly(methacrylic acid-co-acrylamide)/bentonite nanocomposite hydrogels, *J. Polym. Res.*, 29 (2022) 113, doi: 10.1007/s10965-022-02956-0.
- [35] Z. Song, F. Lian, Z. Yu, L. Zhu, B. Xing, W. Qiu, Synthesis and characterization of a novel MnO₂-loaded biochar and its adsorption properties for Cu²⁺ in aqueous solution, *Chem. Eng. J.*, 242 (2014) 36–42.
- [36] W.M. Ibrahim, A.F. Hassan, Y.A. Azab, Biosorption of toxic heavy metals from aqueous solution by *Ulva lactuca* activated carbon, *Egypt. J. Basic Appl. Sci.*, 3 (2016) 241–249.
- [37] S.A. Khan, M.F. Siddiqui, T.A. Khan, Synthesis of poly(methacrylic acid)/montmorillonite hydrogel nanocomposite for efficient adsorption of amoxicillin and diclofenac from aqueous environment: kinetic, isotherm, reusability, and thermodynamic investigations, *ACS Omega*, 5 (2020) 2843–2855.
- [38] M.K. Calik, M. Ozdemir, Synthesis, characterization and swelling behavior of semi-IPN nanocomposite hydrogels of alginate with poly(*N*-isopropylacrylamide) crosslinked by nanoclay, *J. Appl. Polym. Sci.*, 133 (2016), doi: 10.1002/app.43222.
- [39] J. Fabia, A. Gawlowski, M. Rom, C. Slusarczyk, A. Brzozowska-Stanuch, M. Sieradzka, PET fibers modified with cloisite nanoclay, *Polymers*, 12 (2020) 774, doi: 10.3390/polym12040774.
- [40] M. Koosha, S. Hamed, Intelligent chitosan/PVA nanocomposite films containing black carrot anthocyanin and bentonite nanoclays with improved mechanical, thermal and antibacterial properties, *Prog. Org. Coat.*, 127 (2019) 338–347.
- [41] P. Mohammadzadeh Pakdel, S.J. Peighambardoust, R. Foroutan, N. Arsalani, H. Aghdasinia, Decontamination of Fuchsin dye by carboxymethyl cellulose-graft-poly(acrylic acid-co-itaconic acid)/carbon black nanocomposite hydrogel, *Int. J. Biol. Macromol.*, 222 (2022) 2083–2097.
- [42] M.K. Verma, D.E. Nirmal, To study the effect of different salt solution on swelling behaviour of nanoclay polymer composite superabsorbent, *Int. J. Commun. Syst.*, 6 (2018) 768–775.
- [43] H.N. Abdelhamid, Dye encapsulated hierarchical porous zeolitic imidazolate frameworks for carbon dioxide adsorption, *J. Environ. Chem. Eng.*, 8 (2020) 104008, doi: 10.1016/j.jece.2020.104008.
- [44] G.B. Marandi, M. Baharlou, M. Kurdtabar, L. Mahmoodpoor Sharabian, M.A. Mojarrad, Hydrogel with high laponite content as nanoclay: swelling and cationic dye adsorption properties, *Res. Chem. Intermed.*, 41 (2015) 7043–7058.
- [45] S. Madduri, I. Elsayed, E. Hassan, Novel oxone treated hydrochar for the removal of Pb(II) and methylene blue (MB) dye from aqueous solutions, *Chemosphere*, 260 (2020) 127683, doi: 10.1016/j.chemosphere.2020.127683.
- [46] M. Kheirabadi, R. Bagheri, K. Kabiri, Structure, swelling and mechanical behavior of a cationic full-IPN hydrogel reinforced with modified nanoclay, *Iran. Polym. J.*, 24 (2015) 379–388.
- [47] M.V. Nagarpita, P. Roy, S.B. Shruithi, R.R.N. Sailaja, Synthesis and swelling characteristics of chitosan and CMC grafted sodium acrylate-co-acrylamide using modified nanoclay and examining its efficacy for removal of dyes, *Int. J. Biol. Macromol.*, 102 (2017) 1226–1240.
- [48] R. Ghaffari, H. Salimi-Kenari, F. Fahimipour, S.M. Rabiee, H. Adeli, E. Dashtimoghadam, Fabrication and characterization of dextran/nanocrystalline β -tricalcium phosphate nanocomposite hydrogel scaffolds, *Int. J. Biol. Macromol.*, 148 (2020) 434–448.
- [49] A. Mohammadinezhad, G.B. Marandi, M. Farsadrooh, H. Javadian, Synthesis of poly(acrylamide-co-itaconic acid)/MWCNTs superabsorbent hydrogel nanocomposite by ultrasound-assisted technique: swelling behavior and Pb(II) adsorption capacity, *Ultrason. Sonochem.*, 49 (2018) 1–12.
- [50] A. Olad, H. Zebhi, D. Salari, A. Mirmohseni, A. Reyhanitabar, Synthesis, characterization, and swelling kinetic study of porous superabsorbent hydrogel nanocomposite based on sulfonated carboxymethylcellulose and silica nanoparticles, *J. Porous Mater.*, 25 (2018) 1325–1335.
- [51] H. Safarzadeh, S.J. Peighambardoust, S.H. Mousavi, R. Foroutan, R. Mohammadi, S.H. Peighambardoust, Adsorption ability evaluation of the poly(methacrylic acid-co-acrylamide)/Cloisite 30B nanocomposite hydrogel as a new adsorbent for cationic dye removal, *Environ. Res.*, 212 (2022) 113349, doi: 10.1016/j.envres.2022.113349.
- [52] W.F. Lee, Y.T. Fu, Effect of montmorillonite on the swelling behavior and drug-release behavior of nanocomposite hydrogels, *J. Appl. Polym. Sci.*, 89 (2003) 3652–3660.
- [53] S. Abdurrahmanoglu, V. Can, O. Okay, Equilibrium swelling behavior and elastic properties of polymer-clay nanocomposite hydrogels, *J. Appl. Polym. Sci.*, 109 (2008) 3714–3724.
- [54] T. Sharika, A. Mohanan, Synthesis and swelling studies of poly(acrylamide-co-itaconic acid)/hydroxyapatite nanocomposite hydrogels, *Mater. Today Proc.*, 41 (2021) 744–751.